Fermi National Accelerator Laboratory

FN-430
1100.050

A STUDY OF NEUTRON LEAKAGE THROUGH AN IRON SHIELD AT AN ACCELERATOR*

A. J. Elwyn and J. D. Cossairt
Fermi National Accelerator Laboratory, Batavia, Illinois 60510

March 1986

*Submitted to Health Physics

A STUDY OF NEUTRON LEAKAGE THROUGH AN IRON SHIELD AT AN ACCELERATOR

A. J. Elwyn and J. D. Cossairt
Fermi National Accelerator Laboratory, Batavia, Illinois 60510†

ABSTRACT

The spectrum of neutrons, produced in the interactions of hadrons with energies up to several hundred GeV, that are emitted through a large iron electro magnet has been determined by use of a multisphere spectrometer both before and after the shielding was augmented with concrete. The existence of leakage neutrons at energies of ∿0.005-1.0 MeV was verified in the initial configuration, and found to be completely eliminated in the spectrum obtained after the concrete was added. The quality factor of the radiation field was measured; the values are reduced from about six to three with the extra shielding. Additional fluence measurements in the environs of the magnet can be interpreted in terms of a skyshine mechanism with source and attenuation parameters consistent with the energies and intensity of the leakage neutrons.

†Operated by Universities Research Association, Inc.
under Contract with the U. S. Department of Energy

1. Introduction

Alsmiller and Barish (Al73) have pointed out that the neutron spectrum outside of an iron shield should display an excess of neutrons with energies from 0.01 to 1 MeV as compared to the approximately 1/E-shape observed outside of shields composed of materials of lower atomic number (e.g., concrete, soil). The effect arises because of the very small inelastic cross section (Co78) for neutrons in iron at these energies, and the spectral shape predicted by Alsmiller and Barish reflects the presence of resonances (Co78) in the total cross section. Gollon (Go76) has suggested that the existence of these intermediate energy neutrons should markedly affect the quality factor, absorbed dose, and dose-equivalent of the radiation field outside of the shield. Further, as pointed out by both Alsmiller and Barish and Gollon, the moderating effect of light elements will remove these excess intermediate energy neutrons if a sufficiently thick concrete shield is added outside of the iron. (See also Ar69).

Although the effects associated with neutron leakage through iron are well-known, the actual measurement of the neutron spectrum and quality factor of the radiation field in such a situation have not been reported in the literature. During the recent 800 GeV fixed-target running period at the Fermi National Accelerator Laboratory Tevatron, it became possible to study this problem quantitatively when it was found through routine radiation monitoring that a large analyzing magnet associated with an experiment on one of the external beamlines (i.e., ME beamline) was the source of leakage neutrons appearing on the exterior of shielding. This

paper reports the results of measurements of the neutron spectrum and quality factor as well as absorbed dose of the radiation field both before and after the shielding around the magnet was augmented by the addition of concrete. Additional neutron fluence measurements in the environs of this source were also made, and are discussed in terms of a neutron skyshine mechanism (Pa73).

2. Geometry and Absorbed Dose-Rates

Figs. 1 and 2 show several views of the geometrical arrangement of the magnet and associated shielding before and after this shielding was augmented by additional concrete in order to reduce the observed dose-rates in the vicinity. The main change was the addition of 0.91 m of concrete at the position of maximum absorbed dose, with some minor rearrangement of the existing concrete shield blocks. During the running of the experiment, a beam of 800 GeV protons from the Tevatron was targetted on a 0.25 mm thick by 38 mm long horizontally oriented copper plate (not shown). The beam intensity was recorded by a secondary emission monitor (SEM) located 114 m upstream of this target. Sensitive loss monitors verified that essentially all of this beam reached the target. Those protons that did not interact in the target (about 78% of the incident protons), as well as numerous secondary particles produced in the target, entered the aperture of a very large magnet 3.4 m downstream. The magnet, partially shown in Figs. 1 and 2, was 15 m long. The magnetic field in the gap was oriented horizontally so that positively charged particles were deflected downward. At a distance of 1.6 m downstream from the entrance, a copper beam dump (which filled the horizontal aperture and was 0.3 m high) absorbed the rest of the primary beam and a major portion of the secondary particles. The physics experiment downstream from the magnet (to the right - not shown in the Figs.) detected the charged particles deflected by the magnetic field around the beam dump. As seen in the Figs., the particles still within the aperture in the horizontal plane containing the incident beam strike lead bricks, backstopped with polyethylene, near the downstream end. The

interaction of particles with this lead represented the source of the radiation field studied in these measurements. This was verified by observing that the residual radioactivity was localized to that small portion of the lead that could view the copper target directly at a scattering angle at the target of 1.9 degrees. The particles that interacted with the lead represent a broad spectrum of both charged and neutral particles with energies that span the range from thermal up to several hundred GeV.

Fig. 3 shows absorbed doses* at various locations near this neutron source both before and after the placement of the additional shielding. These were obtained with a commercial tissue-equivalent proportional chamber† which responds to all components of the radiation field. The measurements were taken at a distance of $\sim$0.9 m above the concrete floor of the enclosure. It is clear from Fig. 3 that the intensity of the radiation field was peaked at the location at which the large magnet was viewed directly. Note that the absorbed dose at this position was reduced by a factor of 22 after the concrete was added.

*The values are absorbed dose, but also represent (approximate) hourly absorbed dose-rates during routine operation.

†Health Physics Instruments, Model 1010, Health Physics Instruments, Inc., 1920 Chapala Street, Santa Barbara, CA. 93101.

3. Neutron Spectrum Measurements

The spectrum of the neutrons that leak through the shielding was determined, at the locations indicated in Figs. 1 and 2, by use of a Bonner multisphere spectrometer (Br60; Aw85). This is a low-resolution system that consists of scintillation crystals surrounded by moderating polyethylene spheres of radii 25.4, 38.1, 63.5, 102, 127, and 152 mm.† The scintillators were 8 mm diameter by 8 mm long ^{6}LiI(Eu) crystals, sensitive to thermal neutrons through the ^{6}Li (n, α) ^{3}H reaction, embedded in small (12.7 mm diameter by 12.7 mm long) cylinders of plastic scintillator. This phoswich detector has been described previously (Aw73; Co85b). For present purposes it is sufficient to point out that standard electronic techniques were used to separate the slow pulses due to the ^{6}Li interactions from the fast signals associated with the plastic scintillator, and then to accumulate in a multichannel analyzer only those slow signals that occur in anti-coincidence with the fast pulses. In this manner the peak associated with neutrons appears well separated from charged particle (or other) background events in the pulse-height spectrum.

The phoswich scintillator was placed in the center of each polyethylene sphere consecutively at a position about 3.2 m from the base of the magnet. A measurement was also made with a bare (unmoderated)

†A 229 mm radius sphere normally used in such measurements was not utilized in the present work.

detector. The electronics were gated-on only during the 23-sec beam spills, and a tissue equivalent ionization chamber called a CHIPMUNK (Aw72) placed adjacent to the spherical detector provided the relative normalization for the individual measurements. In general, the phoswich counting rates were sufficiently small that deadtime corrections were negligible. The measured detector responses normalized so that their sum is unity are shown in Fig. 4 for the runs without and with the additional shielding. The solid curves are fits based on an assumed neutron spectrum, as discussed below.

The measured neutron counts C_r are related to the differential neutron fluence N(E) (i.e., the neutron spectrum) through the equation

$$C_r = \int_0^\infty N(E)\ R_r(E)dE, \qquad (1)$$

where $R_r(E)$ is the energy-dependent response function for a sphere of radius r. Given C_r and R_r, N(E) can be obtained by standard unfolding techniques. It is well known (Ch83; Co85b; Ro85) however that such multisphere unfolding has inherent difficulties because of its underdetermined nature. In the present work, the range from thermal energies up to a few hundred MeV is divided into 31 energy bins so that with only 7 detectors the unfolding problem requires the solution of 7 equations in 31 unknowns. This difficulty manifests itself as more than one solution spectrum that can describe the data equally well.

Two different computational techniques have been used in order to gain some confidence in the reasonableness of the unfolded spectrum: SWIFT (OB81; OB83; Ch83; Ro85) is a computer program based on a Monte Carlo method and allows a broad sampling of possible neutron spectra with no a priori assumptions about their character. BUNKI (Lo84) uses the SPUNIT (Br84) interactive recursion procedure along with an algorithm that allows different starting solutions. The resultant SWIFT spectrum is an average of the 100 best-fit spectra from the approximately 7×10^6 sampled. For all cases studied with SWIFT the results tend to be less smooth functions of energy then are those from BUNKI; in some cases spectral peaks appear that are narrower than the expected resolution and thus less physically reasonable. For both programs the response functions R_r for each sphere are those of Sanna (Sa73) appropriate to 8 mm diam. by 8 mm long ^{6}Li(Eu) crystals.

The unfolded spectra based on the fits shown in Fig. 4 are displayed in Fig. 5. Note that the energy scale is logarithmic and the ordinate is $N(E)/\Delta(\log E)$ so that the area under the curves for each energy bin is proportional to the neutron fluence within that bin. The unfolded spectra associated with the situation before the concrete shield was added are very similiar for both computer programs. The characteristic feature in both cases is the peak at energies between $\sim$0.005 and 1 MeV, corresponding to neutrons that leak through iron, as suggested in (Al73). About 55% of the total fluence arises from neutrons with energy greater than 1 keV, with $\sim$60% of this amount (or 33% of the total) from those with energies greater than 50 keV. This is to be compared with the results after 0.91 m of

concrete shielding was added. The excess intermediate energy neutrons are almost completely gone. The BUNKI results show that only 18% of the fluence arises from neutrons with energy greater than 1 keV, with only 16% of that number (3% of the total) from neutrons having an energy of 50 keV or higher. It is not understood why SWIFT gives a spectrum with a peak near 800-eV. The structure seems to be too narrow to be physically reasonable. Nevertheless it is obvious that even for SWIFT the intermediate energy peak seen in the top part of Fig. 5 is completely eliminated by the added concrete.

The quality factor of the neutron field can be obtained from the spectrum unfolding calculations. As seen in Table 1, the values from the two programs associated with the "before" measurement agree to within about 5%, and the average is about a factor of two higher than the average value "after" the shielding was added. This reflects the higher average neutron energy associated with iron leakage neutrons. The quality factors from spectrum unfolding are in excellent agreement with the values from the completely independent recombination chamber measurements discussed below.

The values of both the neutron fluence and absorbed dose obtained in the calculations also reflect the increase in intensity of intermediate energy neutrons in the configuration before the addition of concrete. In Table 1, the values of fluence and absorbed dose are given per count in the ion chamber (CHIPMUNK) that was used for normalization. The numbers in rows 4 and 8 however are for 10^{12} incident 800 GeV protons and were obtained from the average values (in rows 3 and 6) by normalization of the

CHIPMUNK to the SEM for each of the two running conditions. Although the values of absorbed dose (row 8) differ by about a factor of 4.5 from those obtained with the commercial ion chamber, the ratio for the two different shielding conditions agrees very closely with the ion chamber results.

As mentioned, the spectral measurements were made at a distance of 3.2 m from the base of the magnet. The actual source of neutrons in the magnet is centered at an height of 1.8 m from the floor. Therefore, the distance from the source to the measurement location is about 3.7 m. The fluence 3.92×10^{9} $n\text{-}m^{-2}$ in row 4, Table 1, can be scaled by the inverse square law to give an approximate neutron source strength at the magnet of 5.3×10^{10} neutrons per 10^{12} protons incident on the primary target, or by inverse distance to give a value of 1.45×10^{10} in the same units. The latter extrapolation is perhaps more appropriate since the size of the neutron source within the magnet is the same order of magnitude as the distance from the source to the detector position.

4. Direct Measurement of Quality Factor

In the previous section the quality factor (QF) of the neutron field was determined from calculated values of absorbed dose and dose-equivalent for a given neutron spectrum. We have also performed a direct measurement of this quantity by use of a recombination chamber placed at the same location as for the spectral studies.

The use of columnar recombination to measure the QF of mixed fields of radiation has been described by Sullivan and Baarli (Su63) and summarized by Patterson and Thomas (Pa73). To determine the QF in this manner, the response of a commercial high-pressure ion chamber† specifically designed for this purpose was measured over its operating voltage range ($\leq$ 1200 volts). According to Sullivan and Baarli, the following equation will describe the response of such a chamber,

$$I = kV^N, \tag{2}$$

where I is the measured current or charge collected at the anode at chamber potential V. k is a constant of proportionality dependent upon the chamber used and the absorbed dose rate of the radiation field. The exponent N depends upon the average LET of the radiation present and is thus correlated with the average quality factor. This correlation has been studied previously (Co84; Co85b) by use of radioactive sources to produce

†Model REM-2 Chamber, Radiation Dosimetry Instrument Division, ZZUJ, "Polan," Bydgoszcz, Poland.

radiation fields with QF ranging from unity (^{60}Co γ-rays) to 6.9 (^{238}Pu-Be neutrons and γ-rays), and details concerning the use of the chamber can be found in (Co 84). Fig. 6 in (Co85b) shows the relationship between N and QF based on the calibration measurement with radioactive sources.

In the present measurements, the recombination chamber response was normalized to the response of the commercial ion chamber mentioned in Sect. 2. The measured chamber response along with the values of the QF obtained using the linear calibration relationship seen in Fig. 6 of (Co85b) are shown in Fig. 6. The errors are larger for the responses measured with the additional concrete shield because of the reduced neutron intensity. Both measurements were obtained during a period of about two hours. The values of QF are also listed in Table 1, and are in excellent agreement with the values from the spectral measurements.

The additional concrete shielding reduced the absorbed dose by a factor of 22, and the QF by about a factor of 2. Thus, the dose equivalent was reduced by about a factor of 44. (It is likely that this could have been reduced even further if the augmented concrete shielding was higher in elevation, and placed closer to the magnet). It is interesting to note that the 0.91 m thickness of added concrete should reduce the dose-equivalent for a typical 1/E spectrum by about a factor of ten (Va75). The additional attenuation factor of 4 found in these studies is due to the removal of the excess intermediate energy neutrons from the spectrum.

5. Neutron Skyshine

Although the additional shielding dramatically reduced the neutron fluence, absorbed dose, and dose-equivalent in the immediate vicinity of the magnet, the magnet top and upper parts of the sides remain essentially unshielded by concrete. Neutrons stream out of these source regions into the air, and some are scattered by the atmosphere back to the ground. This scattered component constitutes neutron skyshine (Pa73), and represents a neutron radiation field in the environs of a neutron source even though the direct component is effectively shielded.

A survey was performed at a number of locations near the experimental beamline. The measurements were made along a road that runs approximately perpendicular to the beamline, as seen in Fig. 7. Neutrons were detected by use of a $^{10}BF_3$ precision long-counter (De66) mounted in a vehicle equipped with standard counting electronics. The detector operated as a proportional counter so that use of an integral disciminator sufficed to distinguish thermal neutron capture events due to the $^{10}B(n,\alpha)^7Li$ reaction from a γ-ray or muon-induced process. A microwave telemetry system provided signals to gate on the scalers that register long-counter counts during both beam-on and beam-off time periods. It also transmitted beam intensity information from the SEM in the beamline. Neutron fluence was obtained from measured counting rates after calibration of the long-counter

with an NBS-calibrated ^{238}Pu-Be source.[†]

The product of neutron fluence normalized to 10^{12} incident protons and r^2, where r is the distance to the magnet, is plotted as a function of r in Fig. 8 at the twelve locations at which measurements were made. The error bars on the points are based on combining the statistical uncertainties in the long-counter counts in quadrature with an estimated 12.5% systematic error associated with the long-counter calibration. Plotted in this way the graph shows the departure from an inverse square law. While the data are clearly more consistent with the smooth curve shown than with a straight line, additional measurements at larger distances would have been desirable.

The smooth curve in Fig. 8 is based on a fit to the empirical expression for the neutron fluence due to skyshine (Pa73; Co85a),

$$\Phi(r)=(2.8Q/4\pi r^2)\ [1-\exp(-r/56)]\ \exp(-r/\lambda), \qquad (3)$$

where r is the distance to the source (in m). Q, the neutron source strength, and λ, an effective attenuation length in air, are parameters obtained in the fitting procedure. Their values are indicated in Fig. 8. This expression has been used to successfully describe previous data relating to neutron skyshine for distances $r \geq 50$ m.

[†]Since the long-counter response is uniform for neutrons from about 1 keV up to ~15 MeV, calibration with a ^{238}Pu-Be source (average energy ≈ 4 MeV) should give reasonably accurate counts-to-fluence factors for neutrons that leak through an iron shield.

The value of effective attenuation length λ is dependent on the neutron energy spectrum. Stevenson and Thomas (St84) show that a value λ = 184 m would be consistent with a spectrum that has a maximum neutron energy of a few MeV. This is in agreement with the expectation that the observed neutrons are predominately those associated with leakage through the iron magnet. The intensity of such neutrons, the neutron source strength Q, has a value from the fit (1.75×10^{10} neutrons per 10^{12} protons) that falls within the range 1.45×10^{10} - 5.3×10^{10} neutrons per 10^{12} protons inferred from the spectral measurements described in Sect. 3. Actually, since the extra shielding around the magnet reduces the area of the source, the neutron intensity should be somewhat lower than what it was during the initial spectrum measurement.

6. Summary

Spectral measurements have verified the prediction that neutrons with energies between about 1 keV and 1 MeV leak through an all-iron shield, and that the addition of about 0.9 m of concrete in back of the iron almost completely removes them. The strength of this source of intermediate energy neutrons can be inferred from these measurements and is consistent with the value found from an analysis in terms of a neutron skyshine mechanism of other fluence determinations made in the environs of this source. Further, direct measurements show that the quality factor of the radiation field outside of the shielding is reduced by a factor of two when concrete blocks are added in back of the all-iron configuration.

REFERENCES

(Al73) Alsmiller Jr. R.G. and Barish J., 1973, "Shielding against the neutrons produced when 400 MeV electrons are incident on a thick copper target," Particle Accelerators 5, 155.

(Ar69) Armstrong T.W. and Alsmiller Jr. R.G., 1969, "Calculation of the residual photon dose rate around high-energy proton accelerators," Nucl. Sci. and Eng. 38, 53.

(Aw72) Awschalom M., 1972, "Bonner spheres and tissue-equivalent chambers for extensive radiation area monitoring around a 1/2 TeV proton synchrotron," in: Proc. IAEA Symp. on Neutron Monitoring for Radiation Protection Purposes, Vol. 1, p. 297 (Vienna: Int. Atomic Energy Agency).

(Aw73) Awschalom M. and Coulson L., 1973, "A new technique in environmental neutron spectroscopy," in: Proc. 3rd Int. Cong. of IRPA, pp. 1464-1469, U.S. AEC Conf-730907-P2 (Oak Ridge, TN: U.S. Department of Energy, Technical Information Center).

(Aw85) Awschalom M. and Sanna R., 1985, "Applications of Bonner sphere detectors in neutron fields," Rad. Prot. Dos. 10, 89.

(Br60) Bramblett R.L., Ewing R.L. and Bonner T.W., 1960, "A new type of neutron spectrometer," Nucl Instr. and Meth. 9, 1.

(Br84) Brackenbush L.W. and Scherpelz R.I., 1984, "SPUNIT, a computer code to multisphere unfolding," in: Computer Applications in Health Physics, Proc. of the Health Physics Society Topical Meeting, Pasco, WA.

(Ch83) Chambless D.A. and Broadway J.A., 1983, "Comments on neutron spectral unfolding using the Monte Carlo method," Nucl. Instr. and Meth. 214, 543.

(Co78) Cohen B.L., 1978, "Nuclear cross sections," in: Handbook of Radiation Measurements and Protection, Section A (edited by A.B. Brodsky), pp. 178-182 (West Palm Beach, FL: CRC Press, Inc.).

(Co84) Cossairt J.D., Grobe D.W. and Gerardi M.A., 1984, Measurements of Radiation Quality Factors Using a Recombination Chamber, Fermi National Accelerator Laboratory, Batavia, IL. 60510, Fermilab Report TM-1248.

(Co85a) Cossairt J.D. and Coulson L.V., 1985, "Neutron skyshine measurements at Fermilab," Health Phys. 48, 175.

(Co85b) Cossairt J.D., Couch J.G., Elwyn A.J. and Freeman W.S., 1985, "Radiation measurements in a labyrinth penetration at a high-energy proton accelerator," Health Phys. 49, 907.

(De66) DePangher J. and Nichols L.L., 1966, A Precision Long-Counter for Measuring Fast Neutron Flux Density, Pacific Northwest Laboratory, Richland, WA. 99352, Report BNWL-260.

(Go76) Gollon P.J., 1976, Dosimetry and Shielding Factors Relevant to the Design of Iron Beam Dumps, Fermi National Accelerator Laboratory, Batavia, IL. 60510, Report TM-664.

(Lo84) Lowry K.A. and Johnson T.L., 1984, "Modifications to Interactive Recursion Unfolding Algorithms and Computer Codes to Find More Appropriate Neutron Spectra," Naval Research Lab, Washington, D.C., 20375, NRL Memo Report 5340.

(OB81) O'Brien K. and Sanna R., 1981, "Neutron spectrum unfolding using the Monte Carlo method," Nucl. Instr. and Meth. 185, 277.

(OB83) O'Brien K. and Sanna R., 1983, "Reply to Chambless and Broadway," Nucl. Instr. and Meth. 214, 547.

(Pa73) Patterson H.W. and Thomas R.H., 1973, Accelerator Health Physics, (New York; Academic Press).

(Ro85) Routti J.T. and Sandberg J.V., 1985, "Unfolding activation and multisphere detector data," Rad. Prot. Dos. 10, 103.

(Sa73) Sanna R.S., 1973, Thirty One Group Response Matrices for the Multisphere Neutron Spectrometer Over the Energy Range Thermal to 400 MeV, U. S. Atomic Energy Commission, Report HASL-267 (for availability information: U. S. Dept. of Energy, Technical Information Center, Oak Ridge, TN. 37830).

(St84) Stevenson G.R. and Thomas R.H., 1984, "A simple procedure for the estimation of neutron skyshine from proton accelerators," Health Phys. 46, 115.

(Su63) Sullivan A.H. and Baarli J., 1963, An Ionization Chamber for the Estimation of the Biological Effectiveness of Radiation, European Organization for Nuclear Research, Geneva, Switzerland, CERN Report No. 63-17.

(Va75) Van Ginneken A. and Awschalom M., 1975, High Energy Particle Interactions in Large Targets, Vol. 1 (Batavia, IL: Fermi National Accelerator Laboratory).

Table 1

		BEFORE	AFTER	
NEUTRON FLUENCE	BUNKI	8.69	5.47	(10^{6}n-m^{-2})
	SWIFT	8.93	5.69	"
	AVERAGE[a)]	8.81	5.58	"
	AVERAGE[b)]	3.92	0.563	(10^{9}n-m^{-2})
NEUTRON ABSORBED DOSE	BUNKI	1.26	0.32	(10^{-8}Gy)
	SWIFT	1.66	0.32	"
	AVERAGE[a)]	1.46	0.32	"
	AVERAGE[b)]	6.5	0.32	(μGy)
	HPI-1010[b,c)]	1.4	0.07	"
QUALITY FACTOR	BUNKI	5.30	2.65	
	SWIFT	5.52	2.29	
	AVERAGE	5.41	2.47	
	RECOMBINATION CHAMBER	6.00±0.6	3.00±.27	

a) Values are per CHIPMUNK count
b) Values are for 10^{12} incident protons
c) Commercial tissue equivalent ion chamber. See second footnote in Sect. 2

Figure Captions

Fig 1 Several views of the geometrical arrangement of the magnet and assiciated shielding at the ME beamline before the shielding was augmented with extra concrete.

Fig 2 Several views of the geometrical arrangement of the magnet and associated shielding after the addition of concrete. The additional concrete is indicated by the cross-hatched blocks.

Fig 3 Absorbed dose in $\mu Gy/10^{14}$ protons both before (top) and after (bottom) the placement of the additional concrete shielding. The values are given by the numbers associated with the locations marked by the X's. The added concrete is indicated by the cross-hatched blocks.

Fig 4 Normalized detector response as a function of spherical moderator diameter. The open circles are the measurements before, and the X's are the measurements after the placement of the additional concrete shielding. The smooth curves are calculated results for spectra unfolded using the code BUNKI.

Fig 5 The best-fit spectra before (top) and after (bottom) the placement of the additional concrete shielding, plotted as fluence per unit logarithmic energy interval. The histograms represent the results from the code BUNKI, while the solid points are averages of the 100 best-fit SWIFT spectra.

Fig 6 Recombination chamber response functions measured both before (top) and after (bottom) the placement of additional shielding. Values of the QF are derived from the fitted N-values using the linear relationship shown in Fig. 6 of (Co85b).

Fig 7 Sketch of the environs to the neutron source in the ME magnet, and the locations at which neutron fluence measurements with a precision long-counter were made.

Fig 8 The product of r^2 and neutron fluence $\Phi(r)$ per 10^{12} protons incident on the target as a function of distance from the magnet r in the ME beamline. The smooth curve is a fit to Eqn (3) in the text with parameters λ = 184.4 m and Q = 1.75 x 10^{10} neutrons per 10^{12} p.

Table Caption

Table 1 Neutron fluence, absorbed dose and quality factor from spectra unfolding, and other measurements, both before and after the installation of concrete shielding.

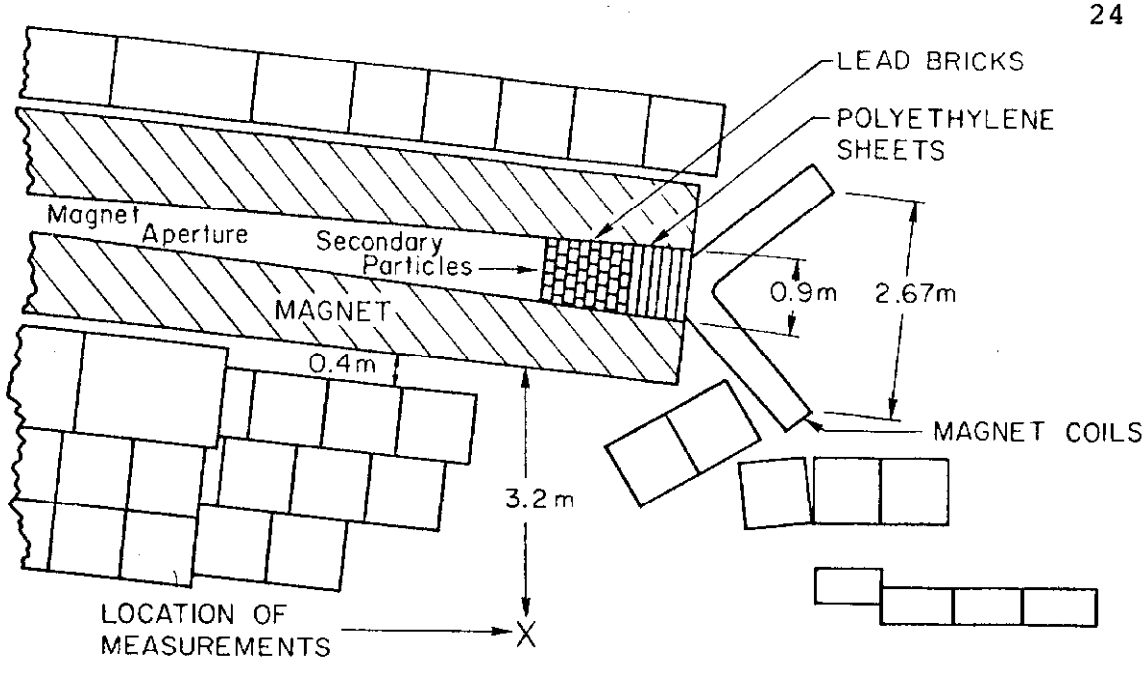

PLAN VIEW IN MAGNET MIDPLANE

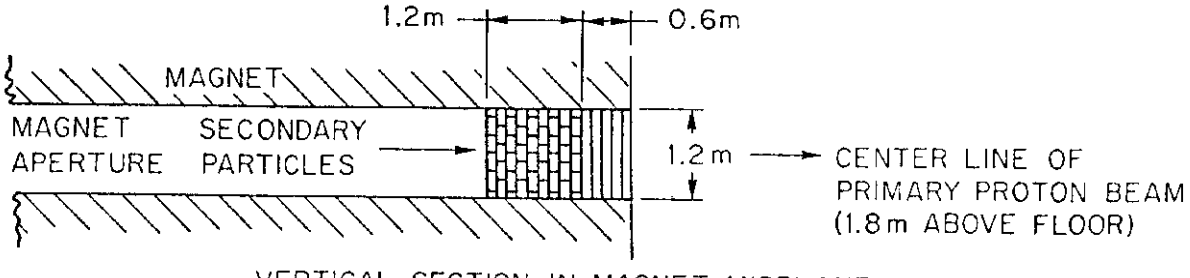

VERTICAL SECTION IN MAGNET MIDPLANE

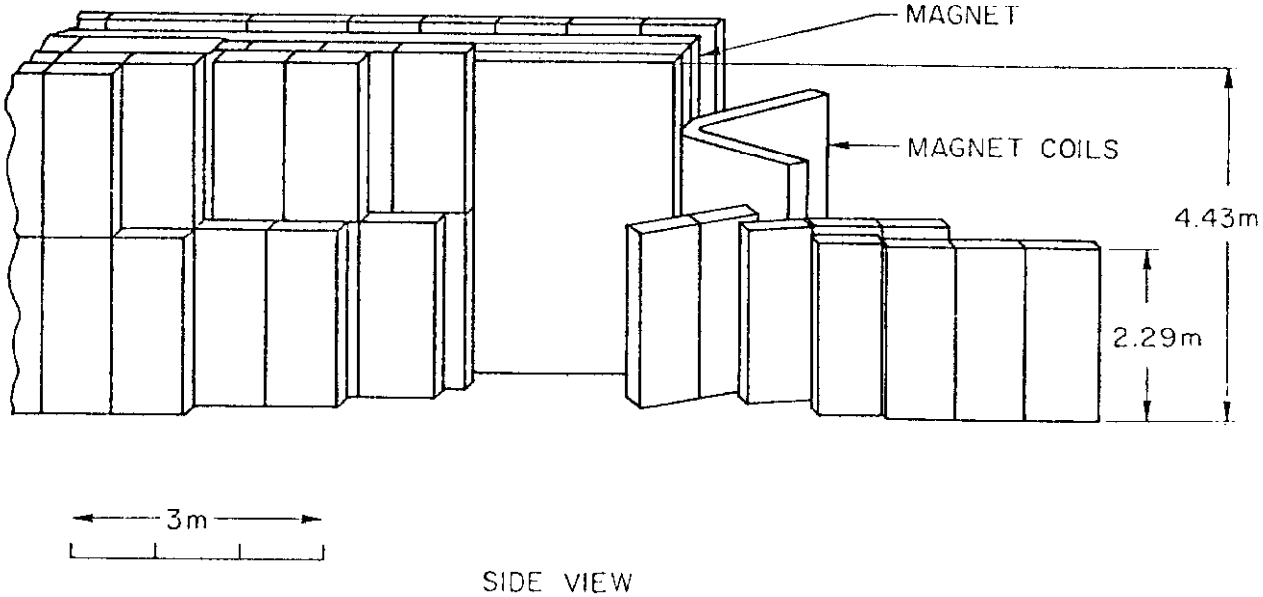

SIDE VIEW

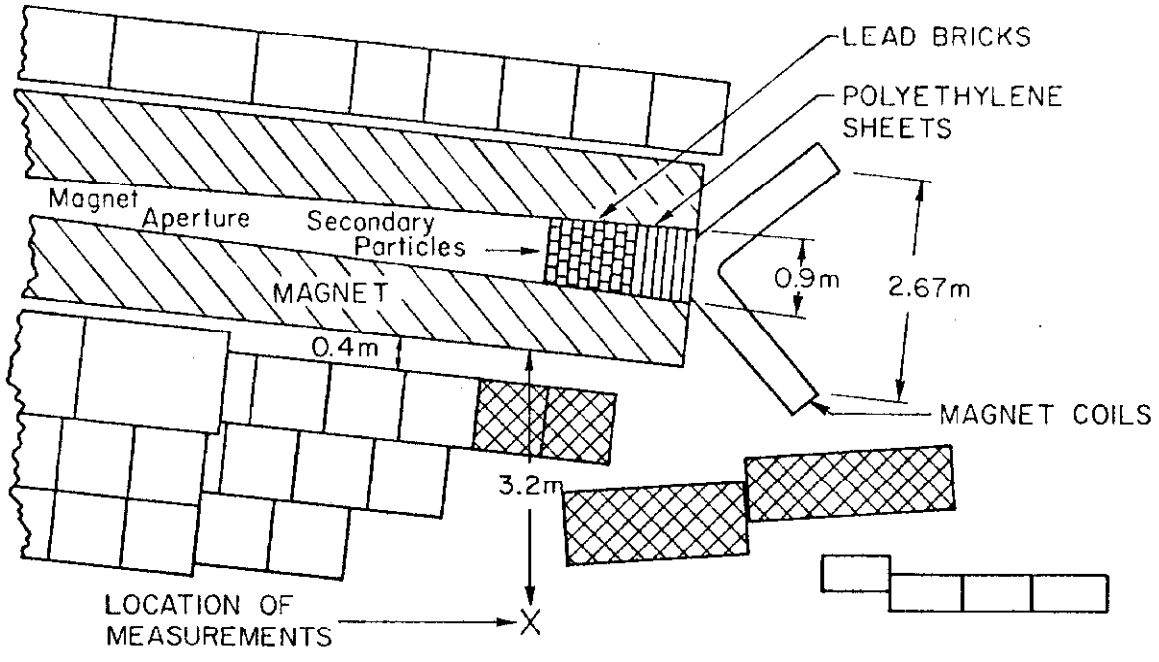

PLAN VIEW IN MAGNET MIDPLANE

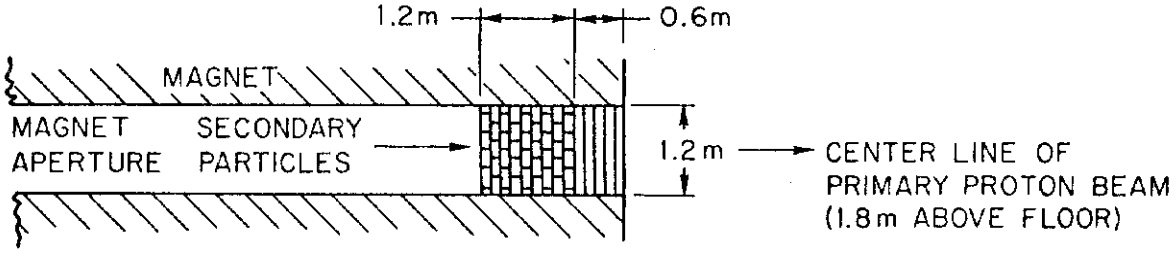

VERTICAL SECTION IN MAGNET MIDPLANE

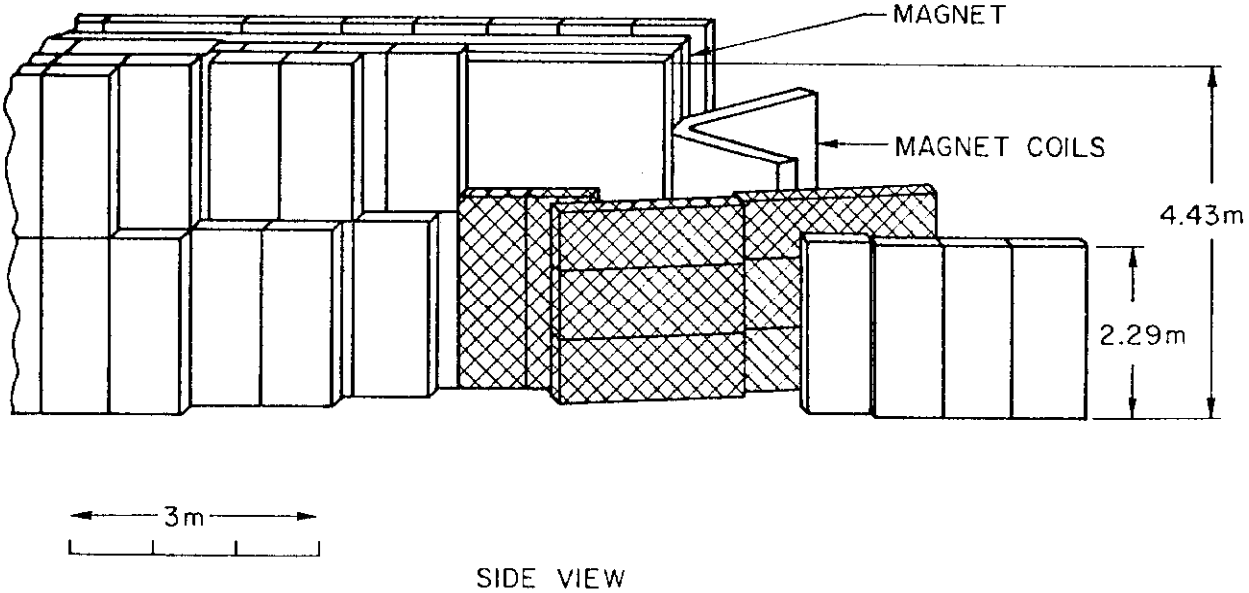

SIDE VIEW

BEFORE

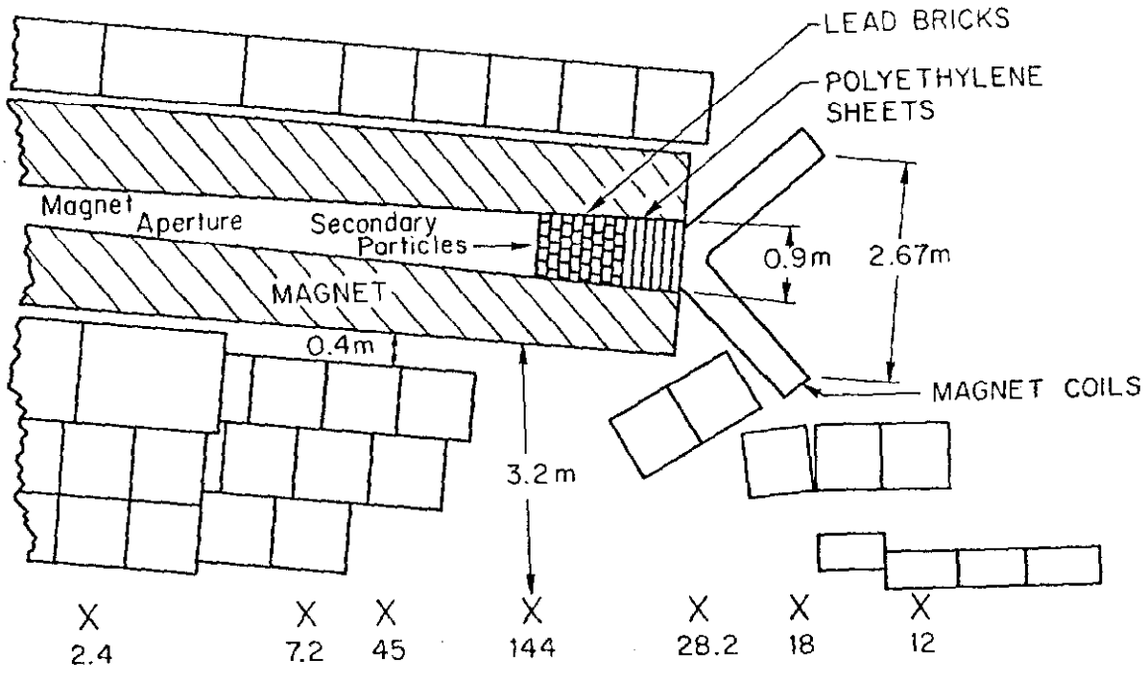

AFTER

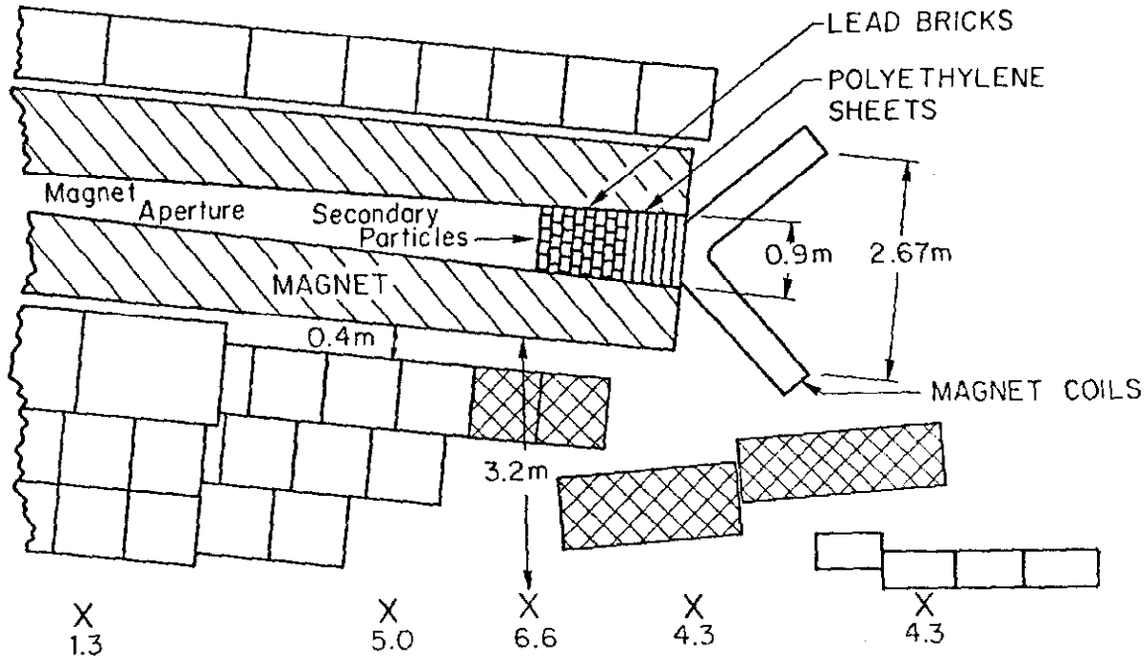

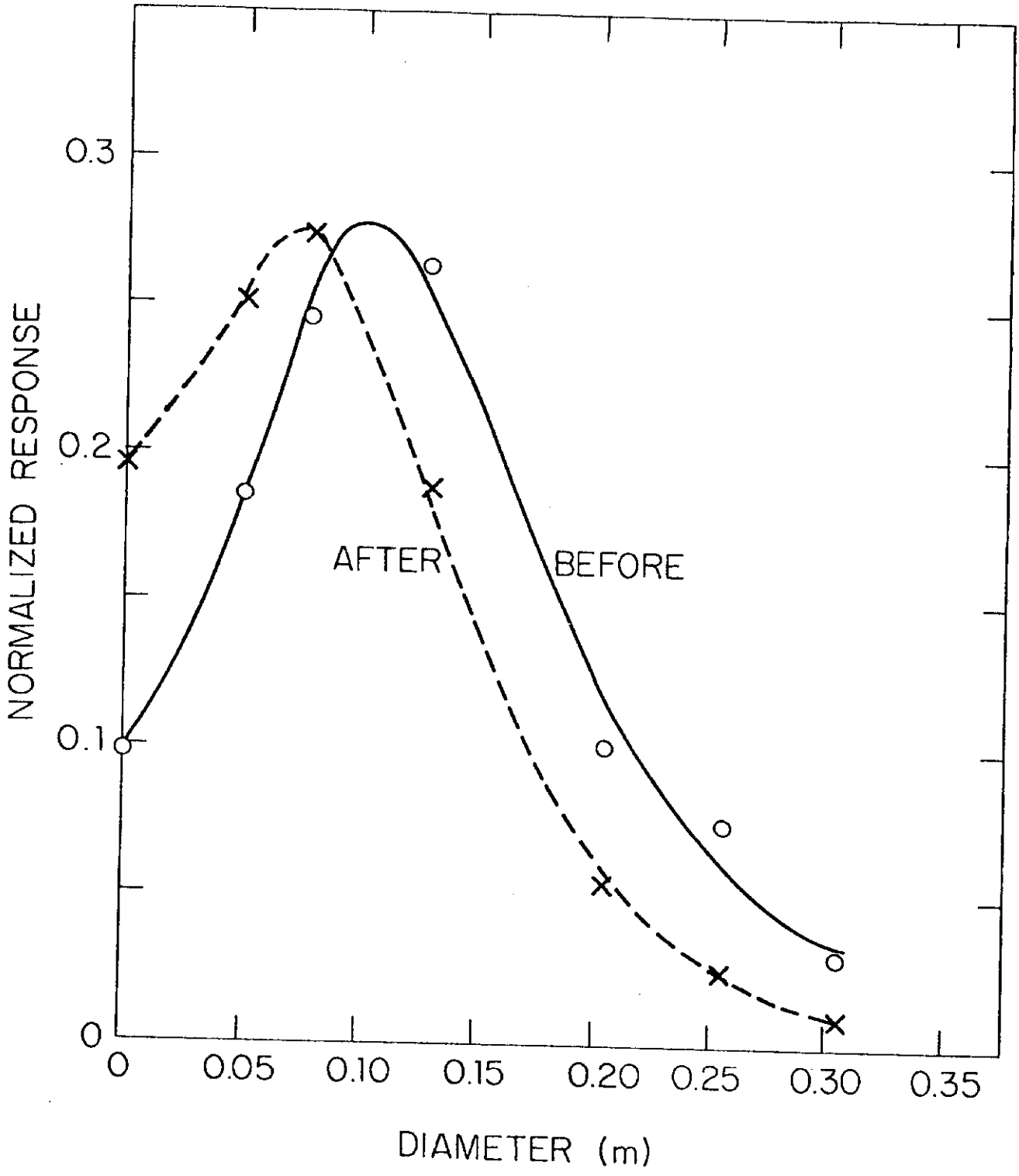
NORMALIZED RESPONSE
0.3
0.2
0.1
0
AFTER
BEFORE
0
0.05
0.10
0.15
0.20
0.25
0.30
0.35
DIAMETER (m)

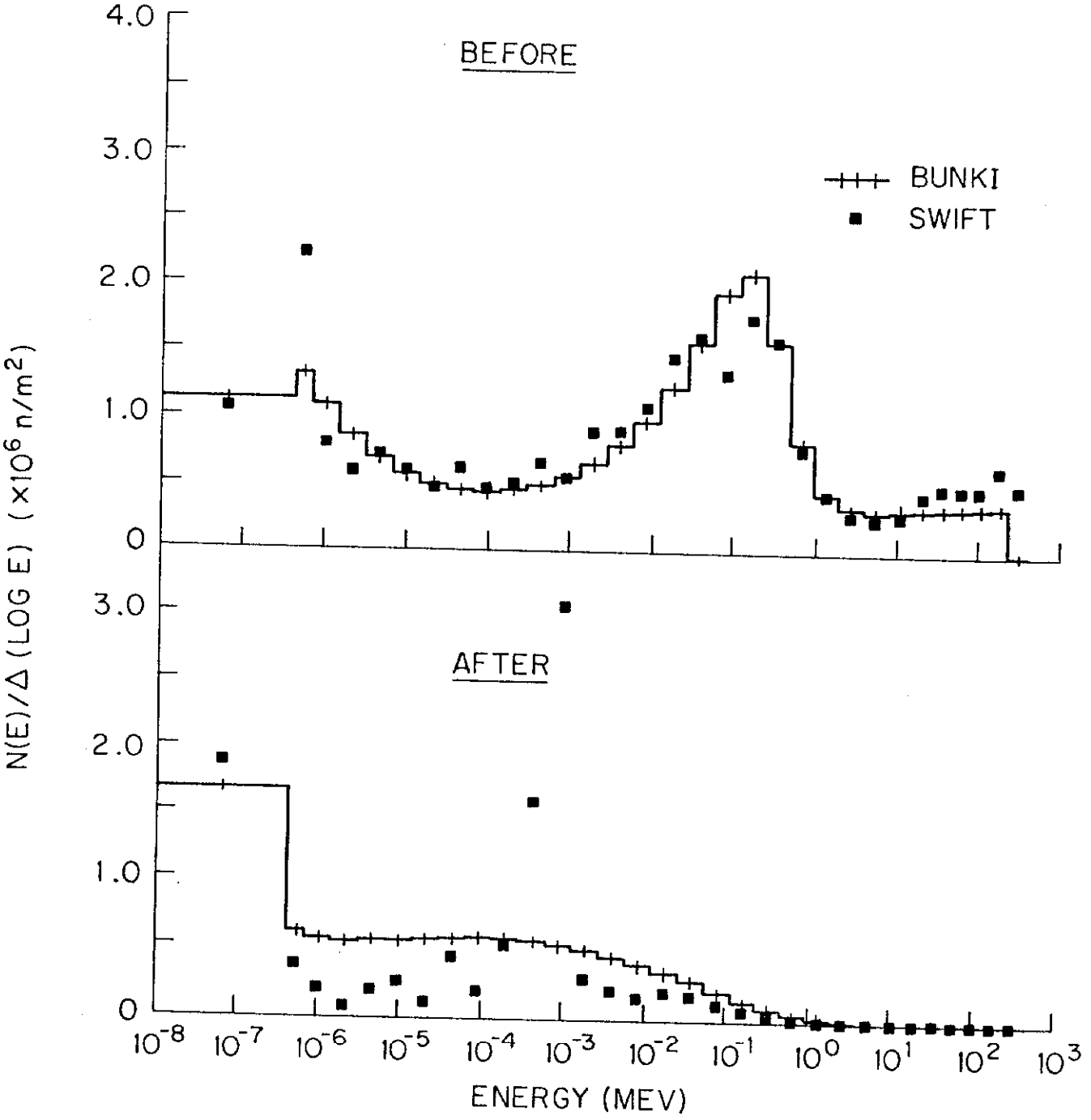
BEFORE
AFTER
BUNKI
SWIFT
4.0
3.0
2.0
1.0
0
3.0
2.0
1.0
0
N(E)/Δ (LOG E) (×10⁶ n/m²)
10⁻⁸ 10⁻⁷ 10⁻⁶ 10⁻⁵ 10⁻⁴ 10⁻³ 10⁻² 10⁻¹ 10⁰ 10¹ 10² 10³
ENERGY (MEV)

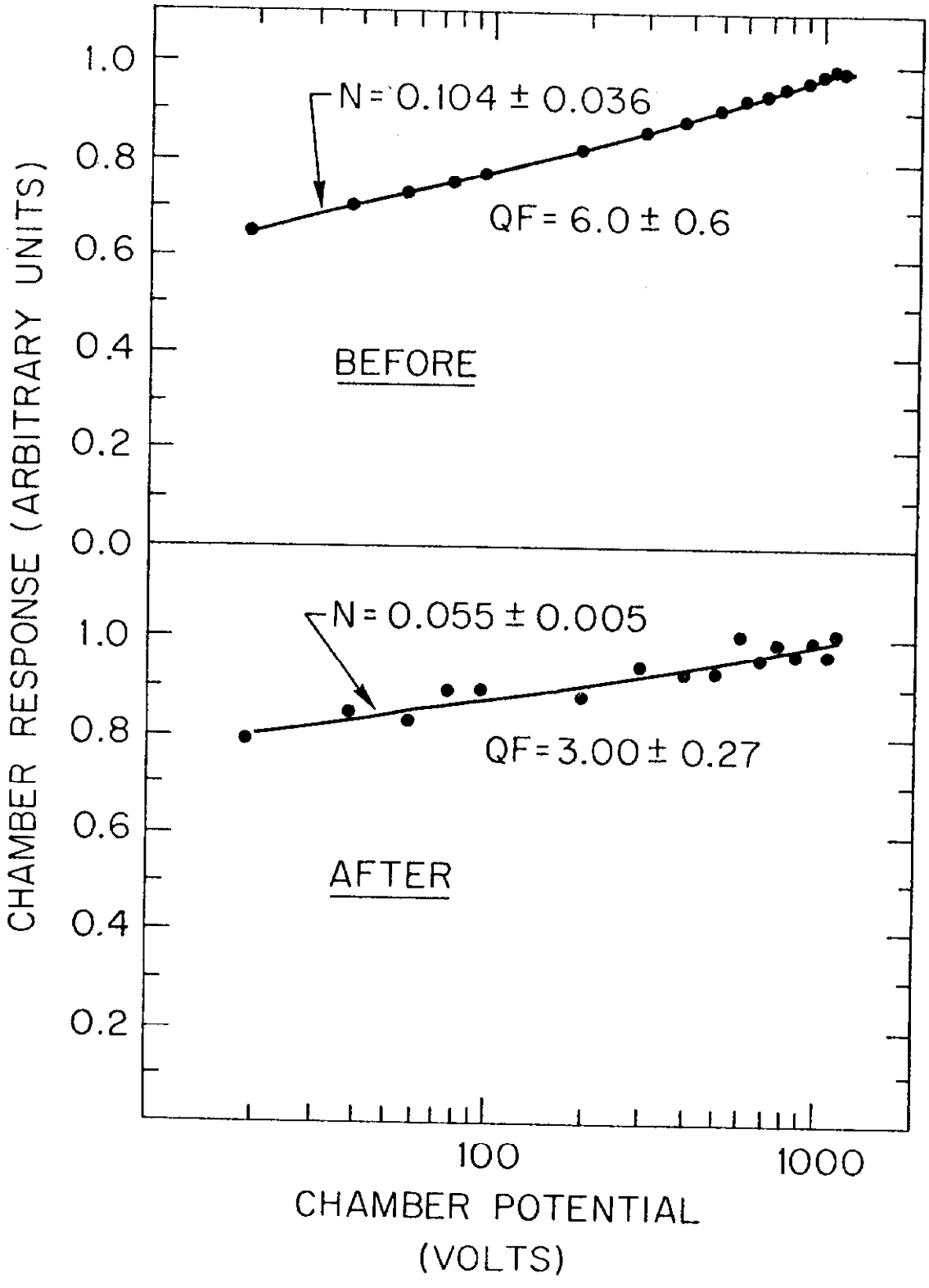
N = 0.104 ± 0.036
QF = 6.0 ± 0.6
BEFORE
N = 0.055 ± 0.005
QF = 3.00 ± 0.27
AFTER
CHAMBER RESPONSE (ARBITRARY UNITS)
1.0
0.8
0.6
0.4
0.2
0.0
100
1000
CHAMBER POTENTIAL
(VOLTS)

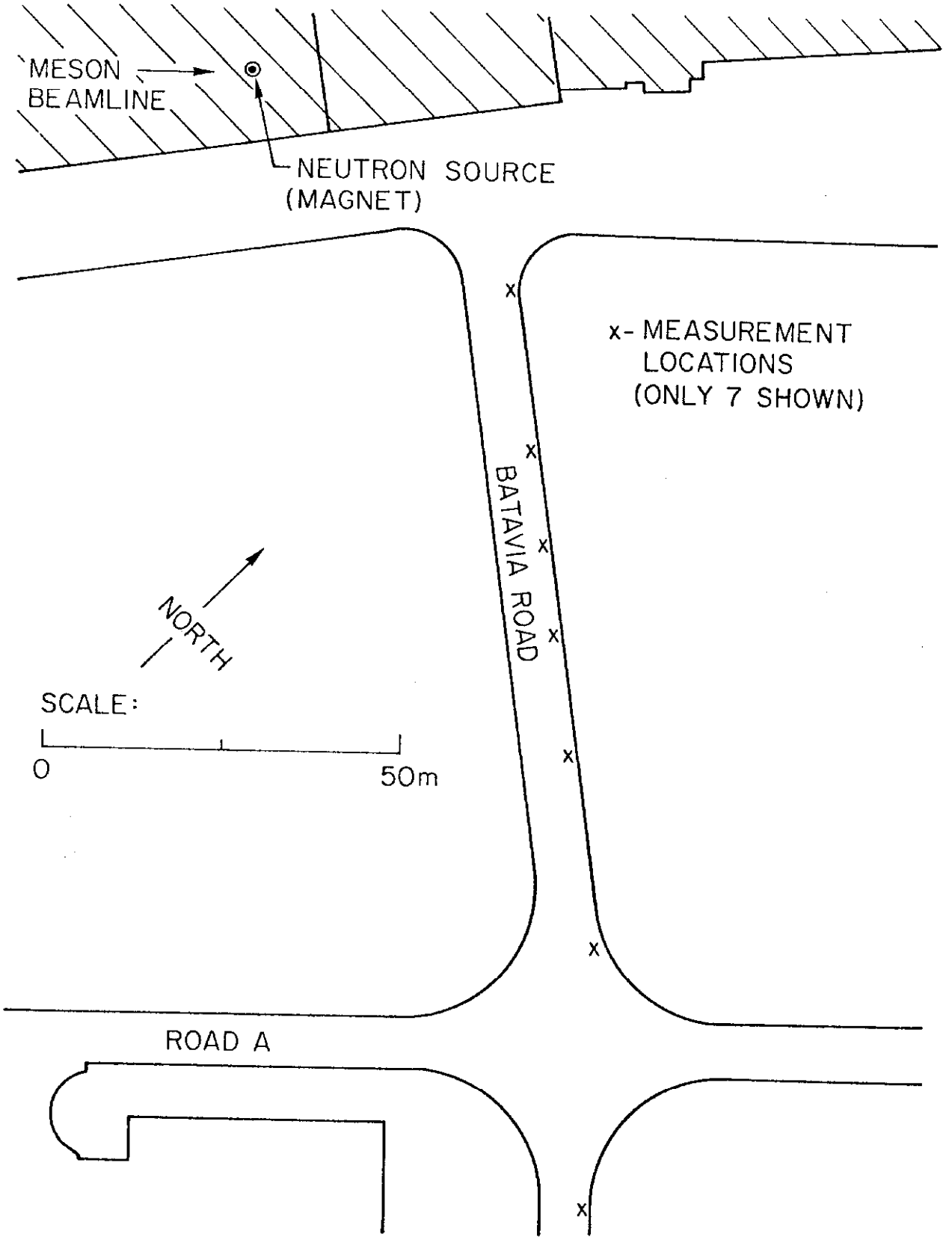
MESON
BEAMLINE
NEUTRON SOURCE
(MAGNET)
x- MEASUREMENT
LOCATIONS
(ONLY 7 SHOWN)
BATAVIA ROAD
NORTH
SCALE:
0
50m
ROAD A

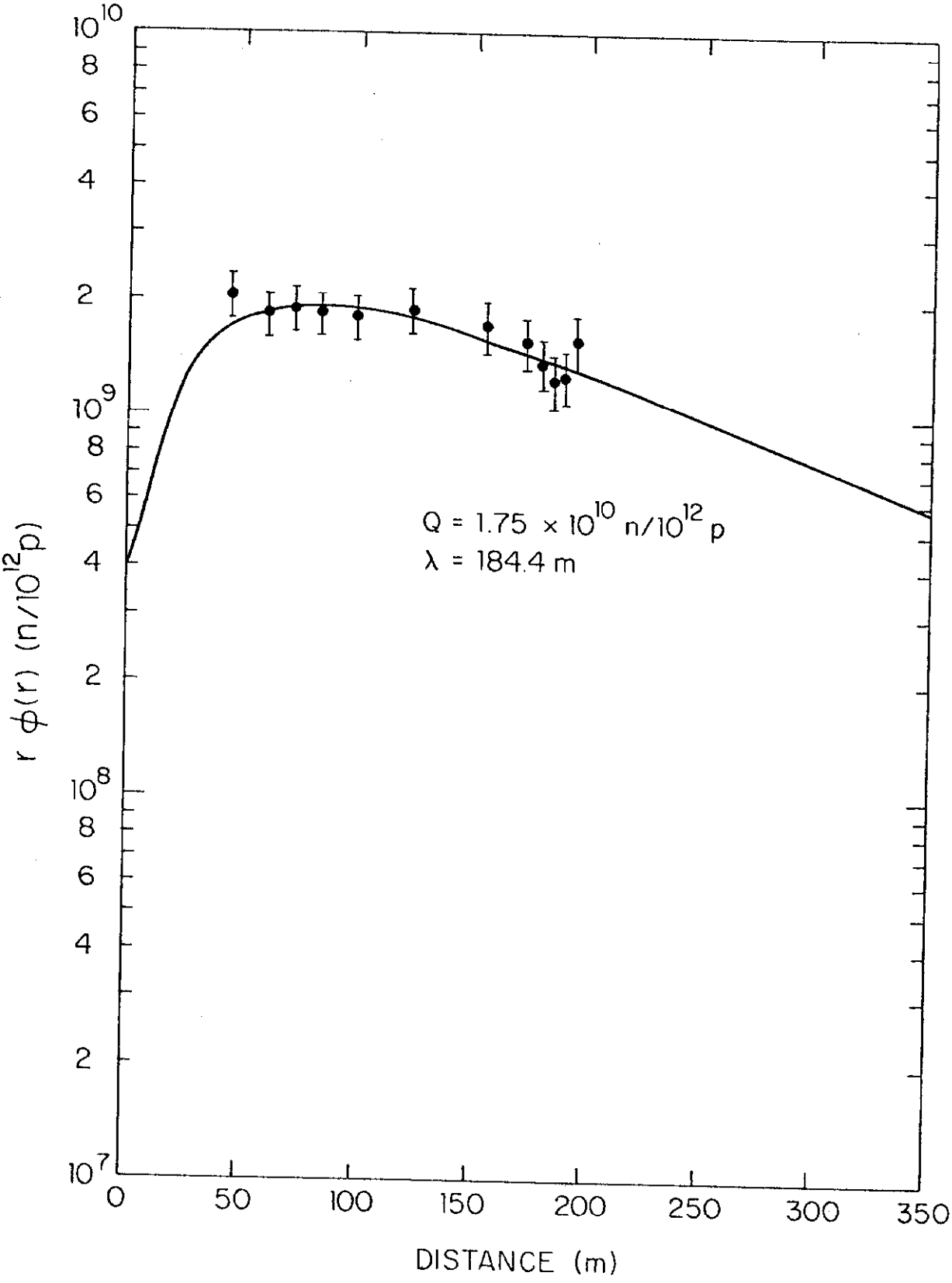
10^{10}
8
6
4
2
10^{9}
8
6
4
2
10^{8}
8
6
4
2
10^{7}
r φ(r) (n/10^{12}p)
Q = 1.75 × 10^{10} n/10^{12} p
λ = 184.4 m
0
50
100
150
200
250
300
350
DISTANCE (m)